SPEED CONTROL OF A VECTOR-CONTROLLED INDUCTION MACHINE USING SLIDING MODE TECHNIQUES IN THE PRESENCE OF NON-LINEAR LOAD DYNAMICS

K.B. Goh, M.W. Dunnigan and **B.W. Williams**

Heriot-Watt University, U.K.
K.B.Goh@hw.ac.uk, M.W.Dunnigan@hw.ac.uk and B.W.Williams@hw.ac.uk

ABSTRACT

This paper presents the application of several control algorithms for speed control of a vector-controlled induction machine in the presence of non-linear load dynamics. Special attention is given to sliding mode control techniques. These techniques provide robustness properties such as external disturbance rejection and good performance with system uncertainty. In order to test the effectiveness of the controllers, several load configurations are used. It is not practical to have a large variety of physical loads. Therefore, the loads are emulated via a particular load emulation technique. The non-linear load under consideration is a single-link robotic arm model with non-linear friction dynamic terms. Three sliding mode control algorithms and a proportional-integral controller are employed for speed tracking control and performance comparison.

1 INTRODUCTION

The objective of this work is to apply robust control techniques for speed control of a vector-controlled induction machine to reduce the effect of non-linear load dynamics. The non-linear load under consideration is a single-link robotic arm and non-linear friction dynamics. The commonly known frictions are viscous, Coulomb, windage, static and Stribeck frictions, Armstrong-Helouvry et al (1). Non-linear load friction control techniques have been reported in the past. Dunnigan et al (2) have used Slotine's sliding mode method (with equivalent control technique) to counter the viscous friction components in an induction machine. Bartolini and Punta (3) proposed a second order sliding mode controller to simulate a mechanical system in the presence of Coulomb friction. Feemster et al (4) designed an adaptive controller for a second-order mechanical system which incorporates frictional effects such as Coulomb, static, Stribeck and viscous friction.

It is impractical to have numerous different physical loads in the research laboratory. Thus, a load emulation technique is used in the work to emulate the non-linear load dynamics. The emulation technique by Hakan et al (5)(6) is adopted in this paper and is used to emulate the single-link robot arm and the non-linear friction dynamics. This configuration is useful for determining basic system performance metrics such as tracking performance and control signal activity under non-linear load conditions.

In this paper, attention is given to sliding mode control techniques. These techniques are well known for their robustness properties and the controller design is relatively straightforward. Utkin (7), Zinober (8) and Edwards and Sarah (9). Several control schemes (i.e. Slotine's SMC, Higher order SMC (HOSM) and pseudo SMC controllers) are considered here. A proportional-integral (PI) control system is also incorporated in the test and the results are used to compare with the SMC controllers performances.

2 MODELLING OF SINGLE-LINK ROBOTIC ARM

Consider a single-link robotic arm in Figure 1.

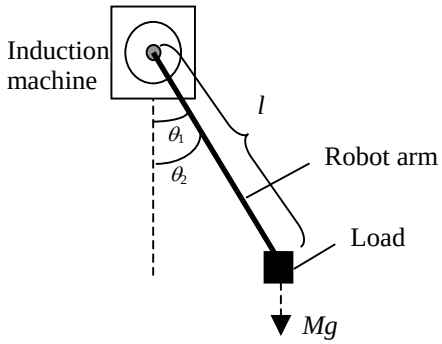

Figure 1: Single link robot arm.

It is assumed the mass of the robot arm is *m* and is evenly distributed. A load with mass of *M* is attached to one end of the robot arm. The equation of motion for the arm is:

$$J\frac{d^2\theta_1}{dt^2} + B\frac{d\theta_1}{dt} + T_{arm} + T_L + T_{NL} = T_e \qquad (1)$$

$$T_{arm} = J_{arm}\frac{d^2\theta_2}{dt^2} + \frac{1}{2}mgl\sin\theta_2 + B_{arm}\frac{d\theta_2}{dt},$$

$$T_L = J_L\frac{d^2\theta_2}{dt^2} + Mgl\sin\theta_2 + B_L\frac{d\theta_2}{dt}$$

$$J_{arm} = \frac{1}{3}ml^2,\ J_L = Ml^2,\ \theta_1 = \theta_2,\ \frac{d\theta_1}{dt} = \frac{d\theta_2}{dt} = \omega$$

where

T_{arm}	torque of the robot arm [Nm]
T_e	developed torque of the induction machine [Nm]
T_{NL}	torque of the non-linear load [Nm]
T_L	torque of the load [Nm]
J	moment of inertia of induction machine [kgm^2]
θ_1	angular position of the rotor [rad]
θ_2	angular position of the robot arm [rad]

ω angular speed of the machine and robot arm [rad/s]
J_{arm} moment of inertia of the robot arm [kgm^2]
J_L moment of inertia of the payload [kgm^2]
B coefficient of viscous friction on the induction machine [Nms/rad]
B_{arm} coefficient of viscous friction on the robot arm [Nms/rad]
B_L coefficient of viscous friction on the load [Nms/rad]
m mass of the robot arm [kg]
M mass of the load [kg]
g gravitational constant [m/s^2]
l length of the arm [m]

The non-linear friction dynamic term is considered to have windage, coulomb, static and Stribeck friction term as follows:

$$T_{NL} = F_w\omega^2 + \left(F_c + F_s e^{-F_{St}\omega^2}\right)\mathrm{sgn}(\omega) \qquad (2)$$

where F_c, F_w, F_s and F_{St} are coulomb, windage, static, Stribeck friction constants respectively. The signum function in equation (2) is approximated to the following function to avoid simulation difficulty.

$$\mathrm{sgn}(\omega) \cong \frac{\omega}{|\omega| + \delta_{fric}} \qquad (3)$$

where δ_{fric} is a small positive constant. Equation (1) becomes

$$\frac{d\omega}{dt} = \frac{1}{(J + J_{arm} + J_L)}[-\frac{1}{2}mgl\sin\theta_1 - B_{arm}\omega - Mgl\sin\theta_1 - B_L\omega - B\omega - F_w\omega^2 - \left(F_c + F_s e^{-F_{St}\omega^2}\right)\mathrm{sgn}(\omega) + T_e] \qquad (4)$$

3 EMULATION CONTROL SCHEME

The emulation control scheme is shown in Figure 2.

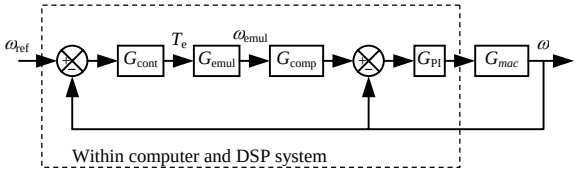

G_{cont} - SMC and PI controllers
G_{emul} - Emulated load. e.g. robotic arm
G_{PI} - PI controller (Iqse current control)
G_{comp} - Inverse of speed tracking loop
T_e - machine torque demand
G_{mac} - Machine system
ω_{emul} - ideal speed demand
ω_{ref} - Reference speed
ω - Output speed

Figure 2: Closed-loop speed control of the robotic arm.

The machine torque is used to drive the emulated load model (e.g robotic arm) G_{emul} to yield a desired shaft speed ω_{emul}. This speed is compared with the measured speed ω. The error is fed through a PI controller, G_{PI} to derive the load torque for the load machine. G_{cont} is the driving machine speed controller (e.g. SMC and PI controllers).

4 SLIDING MODE CONTROLLERS

Three different type of sliding mode algorithms are considered in this paper.

4.1 SLOTINE'S CONTROL TECHNIQUE

A single component version of Slotine's sliding mode control is represented by the following equation, Slotine (10).

$$u = -k_{slot}\,\mathrm{sat}(s/\phi) \qquad (5)$$

$$\mathrm{sat}(s/\phi) = \begin{cases} \mathrm{sgn}(s) & |s| > \phi \\ s/\phi & |s| \le \phi \end{cases}$$

where k_{slot} is a positive constant, $s = \omega_{ref} - \omega$ is the sliding variable, ϕ defines the width of the boundary layer.

4.2 HOSM CONTROL METHOD

The HOSM method generalises the basic sliding mode idea by acting on the higher order time derivatives of the sliding variable instead of influencing the first time derivative as happens in standard sliding mode control. A particular "super twisting" 2-sliding controller, Levant (11), which needs only measurement of s is considered in this paper. It is assumed that upper bounds on the non-linear dynamics are known. The simplified super-twisting algorithm is defined as:

$$u = -\lambda|s|^{\rho}\,\mathrm{sgn}(s) + u_2 \qquad (6)$$
$$\dot{u}_2 = -W\,\mathrm{sgn}(s)$$

where $s = \omega_{ref} - \omega$. This control algorithm does not need any information on the time derivatives of the sliding variable nor any explicit knowledge of other system parameters. Effectively the controller can be tuned via three parameters, ρ, λ and W.

4.3 PSEUDO SMC CONTROLLER

The signum term is commonly used in a sliding mode controller to provide a discontinuous switching effect. It is a single component controller and has the following expression

$$u = -\rho_{\mathrm{sgn}}\mathrm{sgn}(s) \qquad (7)$$

where $s = \omega_{ref} - \omega$ and ρ_{sgn} is a positive scalar. A smoothing factor is introduced in equation (7) as follows

$$u = -\rho_{\text{sgn}} \frac{s}{\|s\| + \delta} \tag{8}$$

where δ is a small positive design constant.

5 SIMULATION AND PRACTICAL INDUCTION MACHINE SYSTEM SETUP

The system uses the standard indirect vector-control technique for torque control. Under perfect tuning, the torque is directly proportional to the torque reference current, i^*_{qse}. The control technique configuration for the test is shown in Figure 3. The data acquisition and control hardware systems consist of a Texas Instrument™ TMS320C6701 DSP board and a PC set. A FPGA AED-106 Multi-channel analog expension daughterboard by Signalware is employed to provide A/D interface, PWM generation and a shaft encoder interface. The generated PWM signals feed through a power inverter which consists of a dc link, six gate drive circuits and a three phase dc-ac IGBT inverter.

The speed reference signal is shown in Figure 4. Figure 5 gives the respective simulated friction dynamic terms and the overall friction dynamics. The friction constants are chosen in such a way that the amplitudes of the respective friction dynamics are distributed equally between ± 0.1 Nm.

6 SIMULATION AND PRACTICAL IMPLEMENTATION RESULTS

The parameter settings for the simulation and practical test are: F_s = 0.0085 Nm, F_w = 6.25 x 10^{-5} Nms^2/rad^2, B = 6.56 x 10^{-4} Nms/rad, F_c = 0.0085 Nm, F_{st} = 0.047, β_{hosm} = 1.0, δ_{fric} = 0.0001, J = 0.06 kgm^2, β_{hosm} = 1.0, ρ = 0.5, k_{slot} = 9, ϕ=0.8, ρ_{sgn} = 9, W = 8.0, λ = 0.1 and δ = 0.01. Figures 6 and 7 show the simulated speed error signal without (T_{NL}) and with non-linear friction dynamics respectively.

The difference between both plots appears at about 0.7s when the machine shaft changes its direction. The Coulomb and Stribeck friction have a more significant effect on the system when direction changes. The speed error increases (comparing between the cases of T_{NL}=0 and T_{NL} present) during the first half and decreases during the second half of the test. This is due to the effective friction dynamic shown in Figure 5.

Several hardware and load emulation configurations are considered in the practical test. Firstly, the emulated robotic arm model is subjected to the speed tracking test. In order to prove the practical validity of load emulation, the inertia of the machine, J, is doubled. To verify the higher inertia load emulation results, a physical flywheel weight is attached to one end of the rotor shaft to increase the effective inertia of the shaft. The resulting machine torque demand, T_e under these tests is shown in Figure 8 (a) to 8(c). The torque demand values of the 'emulated-higher-inertia' system and the 'physical-higher-inertia' vary in the same fashion (compared to the test under T_{NL}=0 condition) in order to drive an effectively higher inertia system. The non-linear friction dynamics are then incorporated in the test. Figure 8 (d) shows the torque demand signal which is relatively higher than the one under T_{NL}=0 condition test. The speed tracking error for this test is shown in Figures 9 (a) and (b). The speed errors from Slotine's and Signum controllers do not vary significantly under both T_{NL}=0 and non-linear dynamic test conditions. The HOSM controller shows small speed error variation. However, the speed error for the PI controller has the largest variation and magnitude error compared to the other controllers. This shows the sliding mode controllers are more robust in rejecting non-linear dynamics and against disturbances such as the non-linear friction dynamics. The PI controller, however, shows a radical speed change and cannot cope with the additional dynamics imposed in the test system. Figures 10 (a) and (b) show the plots of torque demand current value under T_{NL}=0 and non-linear dynamics tests. The torque demand current is relatively larger and more control activity is observed when there are non-linear dynamics presence in the system.

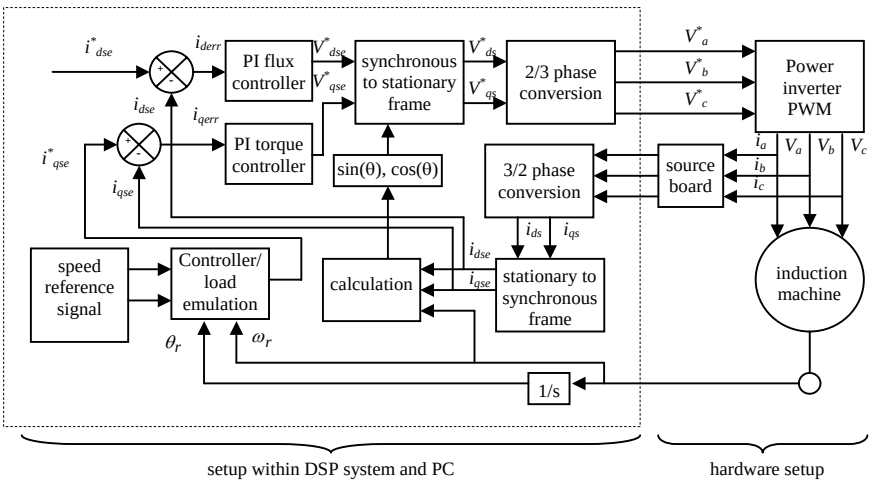

Figure 3: Induction machine test setup.

7 CONCLUSION

This paper has presented the application of sliding mode control techniques for speed control of a vector-controlled induction machine. The performance of the sliding mode controllers under several test conditions have been described, as well as the validation of the load emulation method. The sliding mode controllers, particularly the Slotine and signum implementation, have shown to be robust against non-linear load dynamics variations. This was not seen in the PI controller performances.

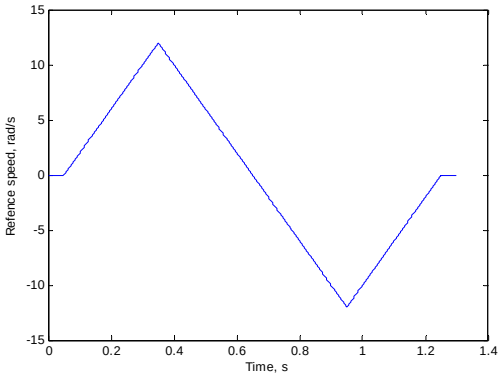

Figure 4: Reference speed.

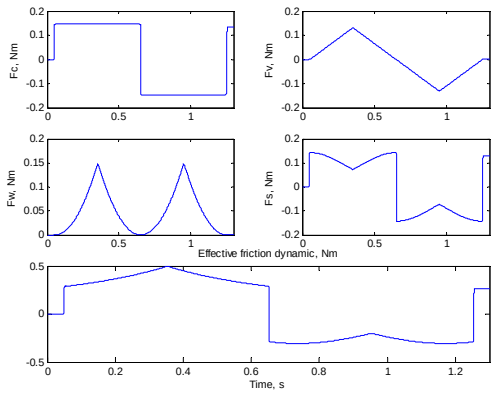

Figure 5: Simulated non-linear friction dynamic.

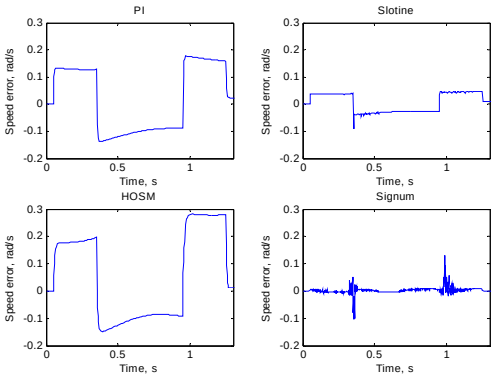

Figure 6: Simulated speed error signal with T_{NL}=0.

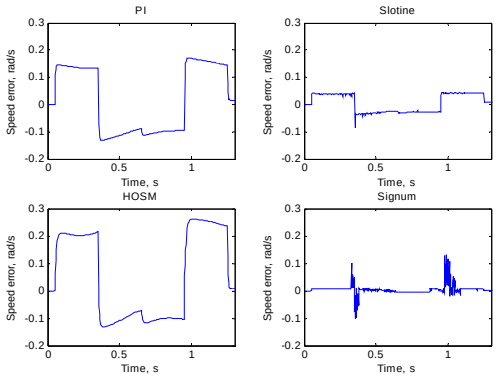

Figure 7: Simulated speed error signal in the presence of non-linear friction dynamics.

8 REFERENCES

1. Armstrong-Helouvry, B., Dupont, P. and Canudas De Wit, C., 1994, Automatica, 30(7), 1083-1138
2. Dunnigan, M.W., Wade, S., Williams, B.W. and Yu, X., 1998, IEE Proc.-Electr. Power Appl., 145(3), 231-238
3. Bartolini, G. and Punta, E., 2000, Journal of Dynamic Systems, Measurement, and Control, 122, 679-686
4. Feemster, M., Vedagarbha, P., Dawson, D.M. and Haste, D., 1998, Proceedings of the American control conference,1488-1492
5. Hakan Akpolat, Z, Asher, GM. And Clare, J.C., 1999, IEEE Transaction on industrial electronics, 46(2) 370-379
6. Hakan Akpolat, Z, Asher, GM. And Clare, J.C., 1999, IEEE Transaction on industry applications, 35(6) 1367-1373
7. Utkin, V.I., 1977, IEEE Transaction on Automatic Control, AC22(2), 212-222
8. Zinober, A.S.I., 1994, "Variable Structure and Lyapunov Control," London: Springer-Verlag.
9. Edwards C. and Spurgeon S.K., 1998, "Sliding mode control: theory and applications," UK: Taylor & Francis.
10. Slotine, J.J.E., 1984, International Journal of Control, 40(2)
11. Levant, A., 1993, International Journal of Control, 58(6), 1247-1263

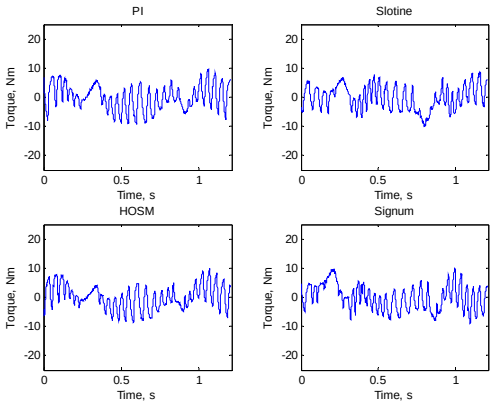

(a)

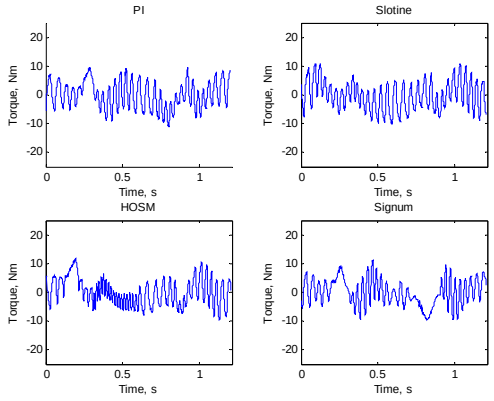

(b)

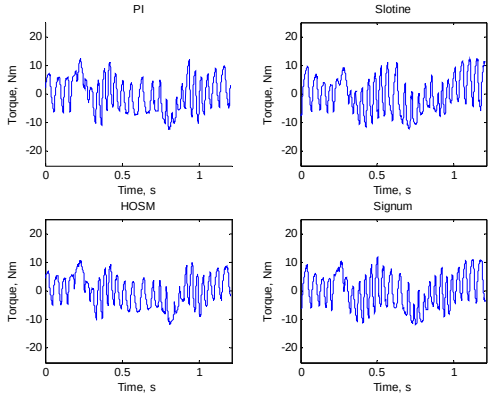

(c)

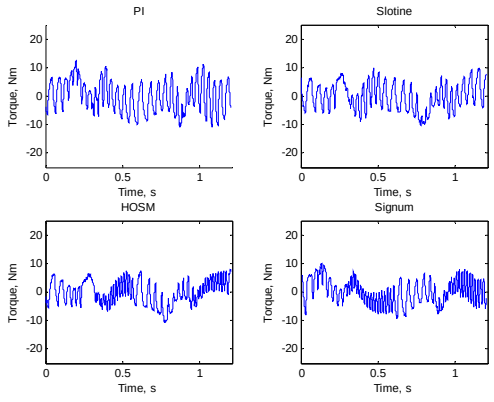

(d)

Figure 8: Plot of machine torque demand, T_e under different testing conditions: (a) when T_{NL}=0, (b) Emulation higher inertia, (c) Physical load inertia and (d) with emulated non-linear friction dynamics.

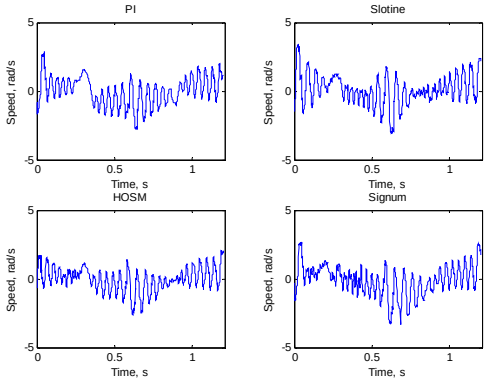

(a)

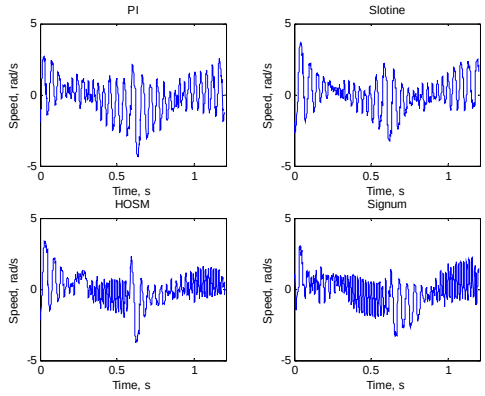

(b)

Figure 9: Recorded speed error: (a) when T_{NL}=0 and (b) with emulated non-linear friction dynamics.

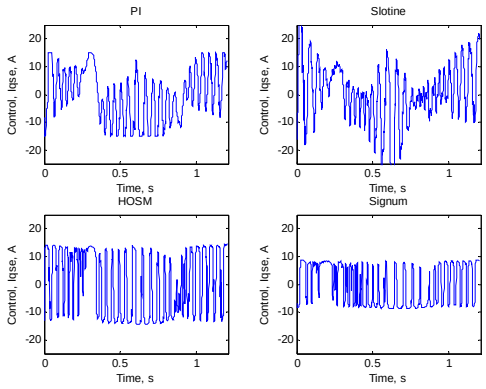

(a)

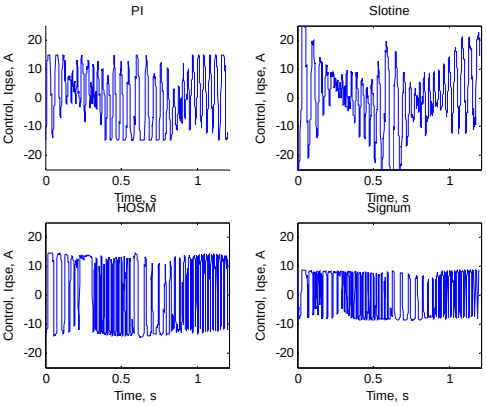

(b)

Figure 10: Recorded torque demand current, Iqse, A: (a) when T_{NL}=0 and (b) with emulated non-linear friction dynamics.